13th International Symposium on Particle Image Velocimetry – ISPIV 2019
Munich, Germany, July 22-24, 2019

Near wake structure of a square back road vehicle

Gioacchino Cafiero*, Juan J. Cerutti, Gaetano Iuso

Dipartimento di Ingegneria Meccanica e Aerospaziale, Politecnico di Torino, Italy

*gioacchino.cafiero@polito.it

Abstract

An experimental investigation focused on the manipulation of the wake flow generated by a square back car model is presented. Four continuously-blowing rectangular slot jets are mounted on the rear base of the model. Dedicated force measurements allowed us to identify a set of configurations leading to significant drag reductions. The maximum drag reduction (12%) is obtained by opportunely tuning the blowing speed of lower and lateral jets only.
An energy budget highlighted the most efficient jet injection accounting for both the drag reduction and the power required to feed the blowing system. Hence, we focused our flow field investigations on two configurations: the maximum drag reduction and the best compromise (yielding 5% drag reduction).
Particle image velocimetry reveals a dramatic change in the wake structure when the control mechanism is actuated in the maximum drag reduction configuration, showing a strong reduction of the streamwise extent of the recirculation bubble behind the model.

1 Introduction

The growing concern on climate problems and the related pollution is pushing all the international institutions to introduce targets for road vehicles' emissions and promoting guidelines for the design of new road vehicles generations. The aerodynamics of the vehicle, especially those with a bluff shape, plays an important role on the vehicle consumption, thus directly influencing the emission of pollutants. Increasing the vehicle aerodynamic efficiency also strongly influences the growing industry of electrically powered vehicles, significantly improving the range and the lifetime of the vehicle.
Passive devices are implemented for a wide range of applications, such as heat transfer enhancement (Cafiero et al. 2016), combustion processes (Geipel et al. 2010) as well as flow control, with particular emphasis on drag reduction (Iuso *et al.*, 2003; Iuso and Di Cicca, 2007; Sardu et al., 2017; Sardu et al., 2015). In the latter case they are massively implemented in road vehicles as well as aircraft and civil structures. Nevertheless, the huge limitation of these devices is their capability of working at the maximum efficiency for one only configuration. Active flow control represents an interesting and appealing alternative. In fact, the possibility of tuning the control parameters on demand to optimize the overall system efficiency in different configurations results to be particularly amenable for practical applications.
Steady jet blowing located near the four edges of a square back model rear base was also studied by Zhang et al. (2018). The model was an Ahmed body presenting a slant angle of 25° on the top edge. The simultaneous application of the four jets led to a dramatic change of the model's drag (quantified in approximately 30%), linked to a strong difference in the flow topology, involving both the extent of the recirculation bubble and the A-pillar vortex originating at the side edges of the model base.
Barros et al. (2016) investigated the implementation of pulsed jets along with Coanda effect. They pointed out that a high frequency actuation is necessary to achieve drag reductions, whilst a

broadband actuation may even lead to drag increments. Furthermore, the effectiveness of the system is even higher when the Coanda effect is exploited, with a smaller entrainment rate in the near wake (even in the steady blowing case) and achieving drag reductions as large as 20%.
An extensive effort has been devoted to the investigation of the flow instabilities arising in the near wake of a square back model. Grandemange et al. (2013) carried out an experimental investigation of the wake bi-stability varying the ground clearance (C/W) for two different values of the model's aspect ratio (H/W=0.74 and 1.34). They showed that, in the case of the Ahmed body (H/W=0.74) for sufficiently large values of the ground clearance (C/W >0.12) the wake exhibits a bi-stability both in the lateral and vertical direction, hence presenting two symmetry breaking modes (SBMs). For H/W=1.34 this is not the case: for all the tested configurations, the flow does not present a bi-stable behavior with respect to the vertical direction, while the lateral one is still present. Volpe et al. (2015), Bonnavion and Cadot (2018) extended these results introducing the effect of yaw and pitch angles. Their results showed that even with a small yaw angle, the onset of a bi-stable behavior in the vertical direction could be detected. More complex is instead the dependency on the pitch angle, where the lateral symmetry breaking mode appears only for a narrow range of angles ($\approx \pm 0.75°$).
Brackston et al. (2016) developed a stochastic model for the suppression of the symmetry breaking mode. Their results, based on the implementation of active flaps near the rear base of the square back model, showed that the mitigation of SBM may lead to drag reduction as large as 24%. Nevertheless, the author pointed out that it was impossible to achieve simultaneous mitigation of the SBM and suppression of wake bistability.
The motivation of this study arises from the general problem of reducing the drag of road vehicles and in particular of a very bluff body configuration (i.e. vans and square-back trucks). Despite the large body of research on this topic, very little attention has been paid to the overall efficiency of the control system. This adds to the available literature aimed at characterize the near wake of a square back model; even if the classic Amhed body has been extensively addressed in the literature, less attention has been devoted to the case with aspect ratio H/W>1 (Grandemange et al. 2013a). Furthermore, a very small number of investigations are interested to more realistic geometries. Hence, we aim at investigating an efficient active flow control technique based on continuous jets applied to a square back 3D van model, using different combinations of the slot jet actuators covering the four edges of the rear base. We assess the effectiveness of the flow control system for a potential realistic application, introducing a definition of the control efficiency which accounts also for the losses in the pneumatic lines. This latter aspect has been often overlooked in previous investigations. To this end, the energy budget analysis is performed in detail and a multi-objective approach is introduced to identify the optimal configurations of the system evidencing a usability map of the control system.

2 Experimental setup

The experiments were carried out in the subsonic open circuit wind tunnel of the aerodynamics laboratory "Modesto Panetti" of the Politecnico di Torino. Air is collected from the surrounding environment using two fans located upstream of the test section. To reduce any bias due to the feeding circuit, air is conveyed through several honeycomb and mesh screen layers. A convergent duct delivers the air to the rectangular test section, whose height (H) and width (W) are 1.2 m and 0.9 m, respectively. Furthermore, the test section is designed with a 1% divergence angle to account for the boundary layer growth on the lateral walls.
The model is a square back road vehicle whose dimensions are chosen to mimic a scale factor of about 1:10 to those commonly employed. This results in a model cross section of height H =0.2 m and width W =0.17 m (see Figure 1a). The rear base of the model presents a taper angle of 10° extending along its entire perimeter. This choice is motivated by the results of Barros et al. (2016)

who showed that the concurrent application of active flow control and Coanda effect is extremely beneficial for the drag reduction purposes.
The model is manufactured in polylactic acid (PLA) plastic through 3D printing. The model's ground clearance h measured with respect to its bottom surface is equal to 20 mm, corresponding to a normalized value $h/H = 0.1$. The model is accurately positioned within the test section 1900 mm downstream the inlet of the test section (total length 6500 mm) through an instrumented strut connected to a balance. The strut hosts the pipelines needed to supply the jets as well as all the electric lines from the sensors allocated inside the model. In order to reduce to a minimum the aerodynamic interference of the strut, it is embedded within a hollow hull with a symmetric airfoil section and a relative thickness $t/c = 0.2$. From the aerodynamic point of view, fixing the four wheels to four load cells positioned under the model outside the wind tunnel would have been a less invasive solution. However, the need of feeding the pneumatic lines with compressed air made us lean towards this solution, albeit more invasive for the flow on the top edge of the vehicle.
The onset of a uniform flow within the test section is obtained by regulating the input shaft power to the fans.

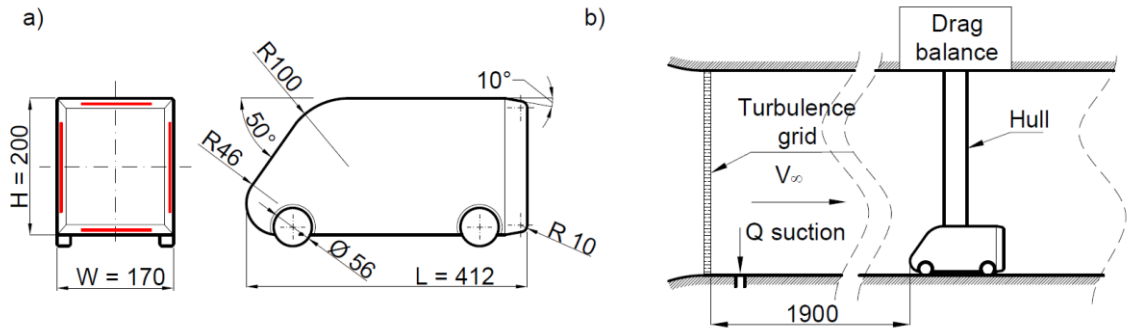

Figure 1: Characteristic model sizes (a) and wind tunnel test section (b). Dimensions are given in mm.

The flow uniformity is further improved by introducing a regular grid with meshlength equal to 65 mm and bar thickness of 20 mm. Furthermore, a suction slot of 250x5mm in located shortly after the turbulence grid near the entrance to the test section (see Figure 1b) to reduce to a minimum the boundary layer growth on the lower wall of the wind tunnel. A vacuum pump provides the flow rate originating a maximum suction velocity of about 15.3 m/s corresponding to a ratio $V_{suction}/V_\infty \approx$ 1.7. We measured the boundary layer investing the model at a distance of 1500 mm from the inlet of the test section and we found that its shape factor is 1.25, with a thickness of nearly 20 mm. Despite the large value of the boundary layer thickness, documented that it mainly affects the lift of the model, whilst its effect on drag is negligible.
The flow speed for all the tests is set to $V_\infty = 9\ m/s$ corresponding to a Reynolds number based on the model length $Re_L = 2.5x10^5$. The corresponding measured drag coefficient C_D= 0.465±5.66E-3 represents well the typical values characterizing the aerodynamics of similar road commercial vehicles.
The wake structure is investigated through PIV measurements. We performed two sets of PIV measurements, aimed at exploring the flow field in planes both parallel to the rear base of the model and the ones aligned with the mean flow direction. The former investigation, which will be referred to as crosswise (CW) case, was carried out at X/W=1. The latter, herein indicated as streamwise (SW) case, at two lateral positions: Y/W=0 and 0.2. A schematic representation of the PIV planes is reported in Figure 2. In the CW case, the laser sheet illuminates a region parallel to the model rear base and extending for 1.18x1 W in the YZ plane, symmetrically located with respect to the XZ

plane. Conversely, in the SW case the laser sheet is aligned to the X axis and covers a region originating from the model base and extending for 1x1.2 W in the XZ plane.
For each location and configuration we acquired 3000 statistically uncorrelated images using one Andor Zyla 5.5Mpix camera equipped with a Nikon 105mm lens. The acquisition frequency is set to 5Hz. The time delay between the two exposures is set to $40\mu s$, resulting in an average particle displacement of 10 pixels. Images of tracer particles are pre-processed to remove the historical minimum, to attenuate the effect of laser reflections on the wind tunnel walls and on the model. Images deformation and velocity vector fields interpolation are carried out using spline functions. A Blackmann weighting window is used during the correlation process to tune the spatial resolution of the PIV process (Astarita, 2007). The final window size is 24x24 pixel (corresponding to 2.5x2.5mm), with 75% overlap. Considering the subpixel accuracy of the PIV process and comparing it to the typical value of the mean flow component in the present investigation we can assess that the average error on the velocity components is much smaller than 1%.

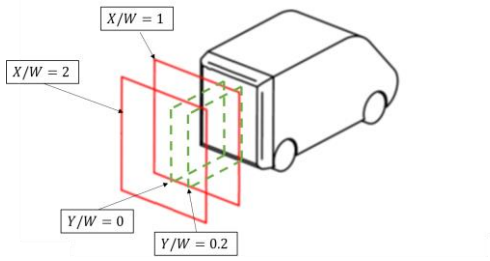

Figure 2: Schematic representation of the PIV system with indication of the imaged planes location.

3 Jets actuation

We performed a parametric study to determine the most favorable configuration in terms of drag reduction, accounting only for lateral (V_{lat}/V_∞) and lower jets (V_{low}/V_∞). It is worth recalling that the lateral jets, in the present experiment, are always activated simultaneously and with the same injection speed. In order to cover a significant portion of the parametric space, we varied the jets' speed in the range $0 < V_j/V_\infty < 1.5$. As evidenced in Figure 3a, high actuation speeds are the most effective in terms of drag reduction as already evidenced in the literature for different vehicle geometries (Barros et al. 2016). It is interesting to notice that, similarly to what already proposed when investigating the single jet actuation, the lower jet is still very effective even with little influence of the lateral jets. However, Figure 3a clearly suggests that the combined effect of lateral and lower jets leads to a drag reduction twice larger than the most favorable standalone configurations. The vehicle's wake is indeed highly three dimensional, hence it is reasonable to expect higher efficiency when acting on the three edges simultaneously, rather than focusing only on the lower part of the wake.
It is worth explicitly mentioning that the blowing jets have a secondary beneficial effect on the drag reduction, given by the thrust that they exert. In Figure 3b we plot the contour representation of the thrust produced by the lower and lateral jets normalized with respect to the drag in the natural case. By comparing Figure 3a and b it is immediate to understand how a large share of drag reduction must be addressed to the effect of the blowing jets at the highest injection speeds. However, their effect is mainly limited to the range of injection speeds $V_{lat}/V_\infty > 1.3$ and $V_{low}/V_\infty > 1$, where T/D exceeds 6%.
Flow control applications in real problems rely on the fact that the proposed solution is efficient in terms of an energy budget. Hence, besides the drag reduction brought by the different configurations, the amount of energy spent to obtain that working condition must be accounted for.

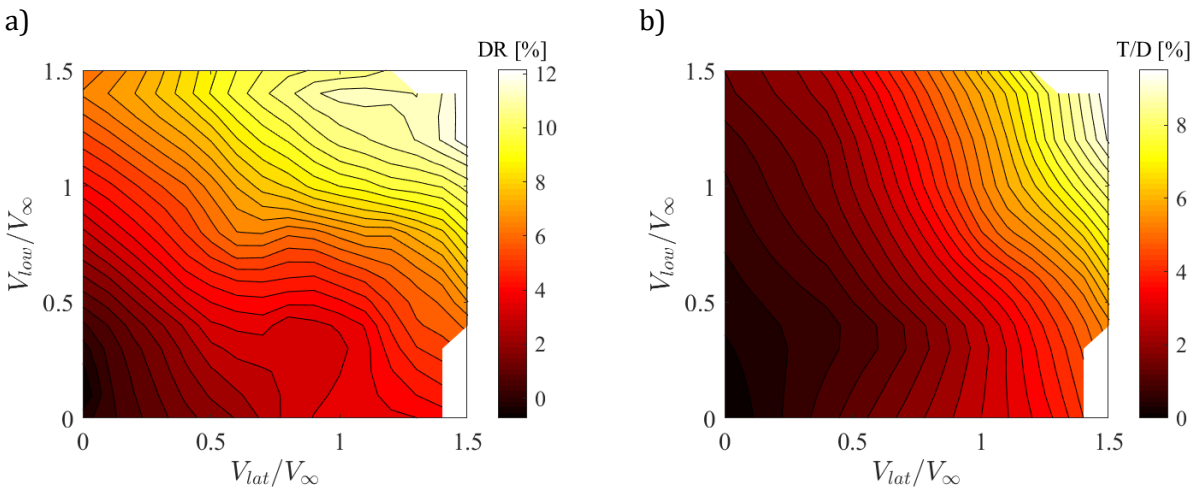

Figure 3: a) Map of drag reduction for asymmetrical forcing. Lower and lateral jet effects. b) Effect of the thrust produced by the blowing jets with respect to the drag of the natural case.

The energy budget was estimated evaluating the energy spent for the flow actuation in terms of losses as well as the corresponding benefit in terms of drag reduction. We introduced the parameter ζ for the global characterization of the efficiency of the system, defined as the ratio between the power saved P_s and the power consumed P_c for the jets actuation.

$$\zeta = P_s/P_c \tag{1}$$

where we define

$$P_s = DR \cdot V_\infty \tag{2}$$

and

$$P_c = (\sum p_{losses}) \cdot Q + \left(0.5\, \rho V_{j_i}^3\right) \cdot A_i \tag{3}$$

whereby A_i we indicate the cross-section of the i-th jet and V_{j_i} the blowing speed of the i-th jet. Equation 3 is obtained by extending the definition given in many previous investigations (Barros et al. 2016, Choi et al. 2008, Zhang et al. 2018) to account also for the losses in the pneumatic line ($(\sum p_{losses}) \cdot Q$). We do this by estimating the losses in the pipings enclosed within the model using empirical relations (Idel'chik, 1960). Even though this approach will lead to smaller values of ζ, it will also give an idea of the energy spent in feeding the jets. It is also important to point out that, as also suggested by Choi et al. (2008), a unique definition of the efficiency of a control system cannot be trivially obtained. The definition proposed here is based on the idea of accounting for all the possible losses that are encountered in a realistic implementation of such control mechanism.
An efficient flow control configuration will be characterized by values of $\zeta > 1$. The sensitivity of this performance parameter is strictly related to some features of the wake receptivity with respect to the forcing and to the optimization of the pressure losses. We did our best to minimize the pressure losses within the model, considering the physical constraints such as the available internal volume. The results are shown in Figure 4 in terms of color map of the efficiency ζ as a function of the velocity ratio of the lateral and lower jets. The pressure drops of each component of the pipe lines were estimated considering the manometers pressure measurements and empirical relations reported in Idel'chik (1960) for all the controlled configurations.

The range of actuation velocities V_{lat}/V_∞<0.5 and 0.5< V_{low}/V_∞ <1.5 is characterized by efficiency values well above unity (whereby V_{lat} and V_{low} are representative of the ejection speed of the lateral and lower jets, respectively). As it can be observed, the effect of the lateral jets for V_{lat}/V_∞>0.5 greatly deteriorates the efficiency for every forcing strength of the lower jet. On the contrary, for V_{lat}/V_∞<0.5 the lower forcing significantly modifies the efficiency evidencing a rather wide region of high ζ.

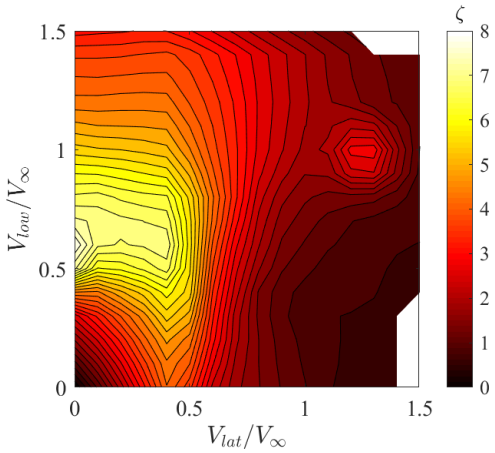

Figure 4: Efficiency ζ of the flow actuation system as a function of the blowing speeds of the lower (V_{low}/V_∞) and lateral (V_{lat}/V_∞) jets.

3 Wake structure

The wake structure is investigated through PIV analysis carried out in two different configurations: one aligned to the streamwise direction, namely along the planes $Y/W = 0$ and $Y/W = 0.2$ that will be referred to as SW case; a second configuration, aligned to the model's rear base along the plane $X/W = 1$ will be referred to as CW case.

Figure 5 shows the contour representation of the mean streamwise velocity component V_x/V_∞ with overlaid streamlines in the XZ plane, measured at Y/W=0, 0.2 for the natural (a, b), best compromise (c, d) and maximum drag reduction (e, f) cases. The streamlines allow for an immediate identification of the streamwise extent of the recirculation bubble originating behind the model's base. In the natural case, at $Y/W = 0$, the bubble extends for about $1.1W$. The interplay between the fluid coming from the model's roof and the high momentum fluid emerging from underneath the model produces a saddle point at $Z/W \approx 0.4$. Furthermore, we can detect two vortical structures: one originating in the vicinity of the model's base, due to the roll-up of the flow leaving the model's roof. The second one caused by the interaction of the nearly quiescent fluid in the model's wake and the high momentum one in proximity of the wind tunnel floor. This structure has been widely documented for similar bodies both experimentally (Grandemange et al. 2013a; Zhang *et al.*, 2018) and numerically (Rao et al. 2018).

The highly three-dimensional structure of the wake, results in a different flow structure as $|Y/W|$ increases. As we move towards the model's side, the recirculation bubble is progressively modified. More interestingly, the two aforementioned vortical regions grow in size: the upstream shift of the unperturbed flow produces a stretching of the upper vortex towards the wake's core. The bottom one instead grows in size as a consequence of the interaction with the flow emerging from underneath the model, which is characterized by higher momentum as we move towards the model's side (hence the unperturbed condition).

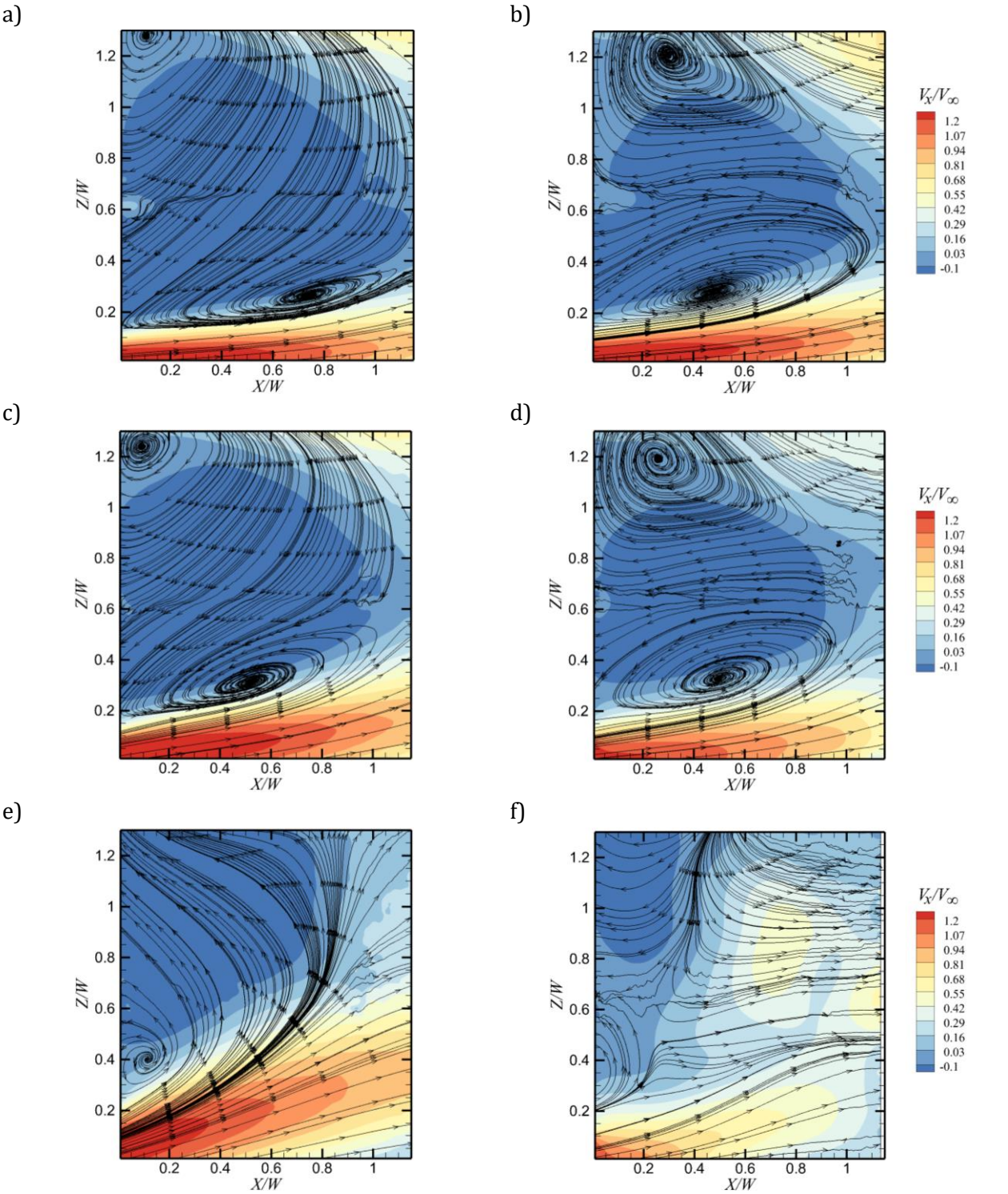

Figure 5: Contour representation of the mean streamwise velocity component V_x/V_∞ in the Natural (a,b), Best Compromise (c,d) and Maximum Drag reduction (e,f) cases (Y/W=0 , left column and Y/W= 0.2 right column).

When the jets are employed in the best compromise configuration, we can detect a reduction of the streamwise extent of the recirculation bubble (nearly 20%) with respect to the natural case. The overall topology of the flow closely resembles the uncontrolled case. The main differences are

limited to the lower vortex: the lower jet produces an upward shift of the vortex, consistently with the reduced extent of the bubble. For increasing values of Y/W, the two vortices undergo an increase in size, in a similar fashion to the natural case.
The maximum drag reduction case features a dramatic change in the mean velocity distribution. The upper vortex disappears, and the mean flow direction within the recirculation bubble undergoes a switch. Furthermore, the high momentum fluid injected through the lower jet, causes a strong reduction of the streamwise extent of the bubble. This is further exasperated when Y/W increases, where the mean flow approaches the unperturbed configuration at streamwise distances as small as $0.5W$.
Figure 6 shows the distribution of the time averaged vertical velocity component V_z/V_∞ at $X/W = 1$ for the natural (a), best compromise (b) and maximum drag reduction (c) cases, with overlaid streamlines. The mean flow structure is progressively affected by the blowing jets, as their strength becomes more and more relevant.
In the natural case, we can detect two large counter-rotating vortices whose extent almost covers the entire model's rear base. The time averaged distribution of the velocity field suggests a vertical asymmetry of the wake, with a preferred shedding direction from the top edge of the model; this result is consistent with the observations of Grandemange et al. (2013b) in the case of an Ahmed body (hence with a preferential shedding out of phase of 90°). The structures, symmetrically located with respect to the XZ plane with the core centered at $Y/W = \pm 0.2$, originate as a consequence of the interaction between the high momentum fluid coming from the model's sides and the one that is forced downwards from the model's roof. These two structures convect downstream and surround the large recirculation region originating in the near vicinity of the model's rear base.
In the best compromise case, reported in Figure 6b, the effect of the lower jet is such that the two vortices are pushed upwards. The result is consistent with the picture depicted in Figure 5, where the model's wake, on average, closes at a larger distance from the wind tunnel floor. The flow topology, underlined using the streamlines, reveals the formation of a saddle point located along the symmetry plane of the model and at $Z/W \approx 0.3$. This represents the most relevant difference with respect to the natural case, where this feature was located closer to the floor, outside of the investigated region.
A dramatic change in the flow field distribution can be instead detected in the MaxDR case. The two large vortices disappear and, even more interestingly, the flow tends towards a nearly symmetric configuration, with a saddle point located in the middle of the imaged area. The disappearance of two vortices, along with the nearly symmetric configuration, suggest a strong suppression of the wake asymmetry when the flow is manipulated in the maximum drag reduction configuration.

4 Conclusion

In this work we carried out the experimental investigation on the effects of an active control system on the wake of a square back vehicle model. The control consisted in four slot jets located near the four edges of the rear base of the vehicle. Different forcing configurations were tested varying the jets strength.
The energy budget analysis highlighted a subset of forcing configurations able to render the wake control profitable form the point of view of potential applications. Differently from previous investigations, we also accounted for the head losses within the pneumatic line that is used to feed the continuous jets. This justifies the difference in terms of the values of ζ found in the present investigation with respect to other investigations (Barros et al. 2016, Zhang et al. 2018 to cite some) where only the momentum flux of the jets is considered.
Among all the favorable configurations, we selected those that were characterized by high values of efficiency ζ. This allowed us to identify two particular configurations respectively referred to as best compromise and maximum drag reduction. The former is characterized by moderate values of drag reduction (nearly 5%) but high values of the efficiency ζ (larger than 4), thus making this solution

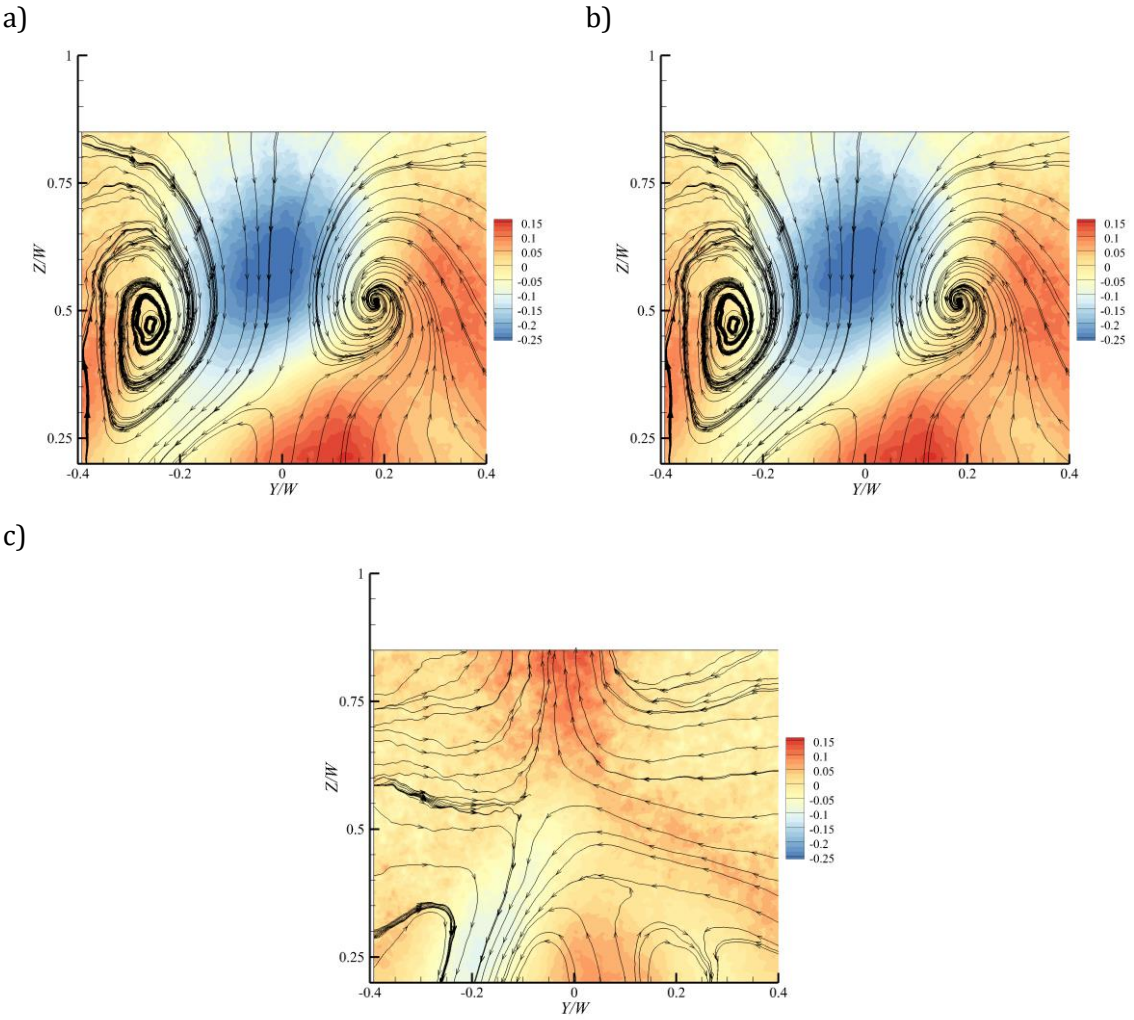

Figure 6: Contour representation of V_z/V_∞ and superimposed streamlines at $X/W = 1$ for the natural (a), best compromise (b) and maximum drag reduction (c) cases. For easiness of interpretation, the car profile is also reported.

particularly amenable for applications; the latter has the maximum achievable drag reduction and unitary values of ζ.

Even with a slightly different geometry of the rear base, presenting slant angles on the four edges, we still retrieve a time-averaged wake structure that is similar to the one presented by other authors in the natural case (Grandemange et al. 2013a; Rao *et al.*, 2018). Two vortical systems are detected: a toroidal structure close to the model base and two large scale streamwise counter-rotating vortices (Rao *et al.*, 2018), produced by the interaction of the flow coming from the top and lateral faces of the model. This wake configuration keeps its main features also for the best compromise forcing, even though the overall length of the recirculation bubble is slightly shortened, while it is completely destroyed in the case of maximum drag reduction forcing.

Acknowledgements

The authors wish to thank Prof. Tommaso Astarita who kindly provided us with the software used to acquire the PIV raw images as well as the one to perform the cross-correlation analysis. The

authors also wish to thank the laboratory technicians Ing. M. Cannata and Mr. M. Grivet for the invaluable help they provided with the experimental setup.

References

Astarita, T. (2007) Analysis of weighting windows for image deformation methods in PIV. *Experiments in Fluids* 43:859-872

Barros D, Borée J, Noack BR, Spohn A (2016) Bluff body drag manipulation using pulsed jets and Coanda effect. *Journal of Fluid Mechanics* 805:422-459.

Bonnavion G, Cadot O (2018) Unstable wake dynamics of rectangular flat-backed bluff bodies with inclination and ground proximity. *Journal of Fluid Mechanics* 854:196-232.

Brackston RD, García de la Cruz JM, Wynn A, Rigas G, Morrison JF (2016) Stochastic modelling and feedback control of bistability in a turbulent bluff body wake. *Journal of Fluid Mechanics* 802:726-749.

Cafiero G, Greco CS, Astarita T, Discetti S (2016) Flow field features of fractal impinging jets at short nozzle to plate distances. *Experimental Thermal and Fluid Science*:78:334–344.

Choi H, Jeon WP, Kim J (2008) Control of Flow Over a Bluff Body. *Annual Review of Fluid Mechanics*, 40(1):113–139.

Geipel P, Goh KHH, Lindstedt RP (2010) Fractal-generated turbulence in opposed jet flows. *Flow, Turbulence and Combustion* 85:397-419.

Grandemange M, Gohlke M, Cadot O (2013a) Bi-stability in the turbulent wake past parallelepiped bodies with various aspect ratios and wall effects. *Physics of Fluids* 25:095103.

Grandemange M, Gohlke M, Cadot O (2013b) Turbulent wake past a three-dimensional blunt body. Part 1. Global modes and bi-stability. *Journal of Fluid Mechanics* 722:51-84

Idel'chik, I. E. (1960) *Handbook of hydraulic resistance (3rd edition)*.

Iuso G, Di Cicca G, Onorato M (2003) Velocity streak structure modifications induced by flow manipulation. *Physics of Fluids* 15:2602.

Iuso G, Di Cicca GM (2007) Interaction of synthetic jets with a fully developed turbulent channel flow. *Journal of Turbulence* 8:11.

Rao AN, Minelli G, Zhang J, Basara B, Krajinovic S (2018) Investigation of the near-wake flow topology of a simplified heavy vehicle using PANS simulations. *Journal of Wind Engineering and Industrial Aerodynamics*. doi: 10.1016/j.jweia.2018.09.019.

Sardu C, Cerutti JJ, Iuso G (2017) Wind tunnel investigation on a squared-back commercial vehicle. in *Proceedings of the 23rd Conference of the Italian Association of Theoretical and Applied Mechanics*.

Sardu C, Sedda S, Iuso G (2015) Drag reduction on a simplified 3D bluff body. in *European Drag Reduction and Flow Control Meeting*.

Volpe R, Devinant P, Kourta A (2015) Experimental characterization of the unsteady natural wake of the full-scale square back Ahmed body: flow bi-stability and spectral analysis. *Experiments in Fluids* 56:99.

Zhang BF, Liu K, Zhou Y, To S, Tu JY (2018) Active drag reduction of a high-drag Ahmed body based on steady blowing. *Journal of Fluid Mechanics* 856:351–396.